Nano Energy 44 (2018) 208–216

Contents lists available at ScienceDirect

Nano Energy

journal homepage: www.elsevier.com/locate/nanoen

Full paper

Managing and maximizing the output power of a triboelectric nanogenerator by controlled tip–electrode air-discharging and application for UV sensing

Gang Cheng[a,b], Haiwu Zheng[b,c], Feng Yang[a], Lei Zhao[a], Mingli Zheng[a], Junjie Yang[a], Huaifang Qin[a], Zuliang Du[a,*], Zhong Lin Wang[b,d,**]

[a] Key Lab for Special Functional Materials, Ministry of Education, Henan University, Kaifeng 475004, China
[b] School of Materials Science and Engineering, Georgia Institute of Technology, Atlanta, GA 30318, United States
[c] School of Physics and Electronics, Henan University, Kaifeng 475004, China
[d] Beijing Institute of Nanoenergy and Nanosystems, Chinese Academy of Sciences, Beijing 100083, China

ARTICLE INFO

Keywords:
Triboelectric nanogenerator
Air discharge
Power management
Self-powered sensors

ABSTRACT

Using a switch has been verified as a promising strategy for managing and enhancing the output performances of a triboelectric nanogenerator (TENG). How to design a switch without external triggering is still a challenge. Here, a self-powered air discharge switch with a tip-plate configuration is developed, in which the switch's on/off state is controlled by the voltage of the TENG itself. The electric output of the TENG can be enhanced and modulated by changing the tip-plate distance of the switch. Compared with the same TENG without a switch, the instantaneous power peak and the total output energy on a load resistance lower than 2 MΩ are increased by 1600 times and 31 times, respectively, as the switch works in an arc discharge mode. It is found that the UV light can change the switch from an arc discharge mode to a corona discharge mode, which increases the equivalent resistance of the switch and decreases the output current of the TENG. The current ratio of this UV detector reaches 18.6, and the lowest detectable light intensity is 26.2 μW/cm^2. Using air discharge switch is a promising route for managing TENG's output power and developing active self-powered UV sensor.

1. Introduction

Recently, triboelectric nanogenerator (TENG) has been developed to convert mechanical energy from environment and human body into electric power [1,2]. Various modes of TENG have been developed by combining contact electrification effect and electrostatic induction effect, which can harvest energy from linear motion [3], rotation [4], vibration [5,6], wind [7,8], water flow [9], rain drop [10] and ocean wave [11,12] et al. In addition, the TENG has already been applied in a wide variety of active self-powered sensors, such as UV light sensor [13], gas sensor [14], chemical sensor [15,16], magnetic sensor [17] and motion sensor [18], et al. However, the TENG has high open-circuit voltage, low short-circuit current, and huge inherently impedance, which bring big challenge for practical applications. For example, when TENG is used to drive electronic devices, the output voltage and power almost drop to zero as the external load resistance is lower than 1 MΩ [19]. Also, when the energy storage device such as a battery or capacitor is used to store the energy of TENG, the storage efficiency is extremely low if directly connected, since there are huge impedance mismatch between the TENG and the energy storage devices [20]. Therefore, managing the electrical output properties is of great importance to TENG's practical applications.

In 2013, the TENG with a switch was reported [21], which has been verified as a key point for TENG's electrical output management. Since the electrical output of TENG can only be generated when the switch is closed, equal output voltage and output energy can be obtained for various load resistances ranging from 500 Ω to 1 GΩ. For a load resistance of 500 Ω, the maximum output voltage and the total output energy of the TENG with a switch are enhanced 5 orders in magnitude, compared with the same TENG without a switch [21]. Through establishing the standards and figure-of-merits of TENG's performances, it is theoretically verified that the instantaneous output power and the total output energy of the TENG can be maximized only when a switch is used [22]. Up to now, the switch has been applied in various modes of the TENG, such as contact-separation mode [21], rotation mode [23], multi-layered mode [24], and two grounded electrodes mode [25].

* Corresponding author at: Key Lab for Special Functional Materials, Henan University, Kaifeng 475004, China.
** Corresponding author at: School of Materials Science and Engineering, Georgia Institute of Technology, Atlanta, GA 30318, United States.
E-mail addresses: zld@henu.edu.cn (Z. Du), zlwang@gatech.edu (Z.L. Wang).

https://doi.org/10.1016/j.nanoen.2017.11.062
Received 17 October 2017; Received in revised form 20 November 2017; Accepted 28 November 2017
Available online 01 December 2017

Recently, various energy management methods based on a switch have been developed [20,26–28], in which the energy storage efficiency as high as 60% can be reached [20]. However, the operations of the switch in these applications are controlled by either external mechanical triggering [21,23–26] or circuit triggering [27,28]. Therefore, the switch has to be elaborately designed to match either the motion or the electrical output of the TENG, which makes the TENG system more complicated and expensive. Designing a self-powered switch without an external mechanical triggering or a circuit triggering is of great importance to developing power management methods of TENG with simple configuration, low cost and high efficiency.

In this paper a self-powered air discharge switch is developed for the TENG, which is composed of a tungsten (W) tip electrode and an adjacent stainless steel plate electrode. Only when the voltage of TENG is high enough for inducing air discharge, the switch is closed and an electrical output is generated. As increasing the tip-plate distance, *d*, the switch is changed from an arc discharge mode to a corona discharge mode. Compared with the same TENG without a switch, the instantaneous output power peak and total output energy in a operation cycle are increased by 1600 times and 31 times, respectively, as the switch works in an arc discharge mode and the external load resistance is lower than 2 MΩ, Also, it is demonstrated that the TENG with an air discharge switch can be used as a self-powered UV light photodetector, in which the current ratio is 18.6 and the lowest detectable light intensity is 26.2 μW/cm^2.

2. Results and discussions

The structure diagram of the TENG with an air discharge switch (TENG-ADS) is shown in Fig. 1. A sliding mode TENG is selected to demonstrate the working mechanism of the TENG-ADS. In principle, the TENG-ADS can be applied in various operation modes of TENG. Two Cu films deposited on a polymethyl methacrylate (PMMA) substrate are served as two electrodes of the TENG, and a polytetrafluoroethylene (PTFE) film with a thickness of 100 μm is served as a triboelectric layer. The PTFE film was treated with reactive ion etching to generated nanostructures on the film surface for enhancing triboelectric properties. The SEM images of the PTFE film before and after etching treatment are shown as Fig. S1 in supporting information. The air discharge switch is composed by two discharge electrodes: a tungsten tip with a curvature radius of 15 μm and a stainless steel plate. These two discharge electrodes are electrically connected with the two Cu electrodes of TENG, respectively. The tip-plate distance, *d*, is precisely adjusted by a micro-manipulation stage. The digital photographic images of the TENG and the air discharge switch are shown as Fig. S2 in the supporting information. As the PTFE film is in contact with Cu electrodes, negative triboelectric charges are generated on the surface of PTFE film due to its more negative triboelectric series [2]. As the PTFE film with negative triboelectric charges horizontally slides, a potential difference between the two Cu electrodes is generated, which is also applied on the air discharge switch to control its on/off states. The air discharge induced by high voltage is a common phenomenon, in which the electrons are accelerated by electric field to bombard and ionize molecules in air [29,30]. As a result, a plasma composed of

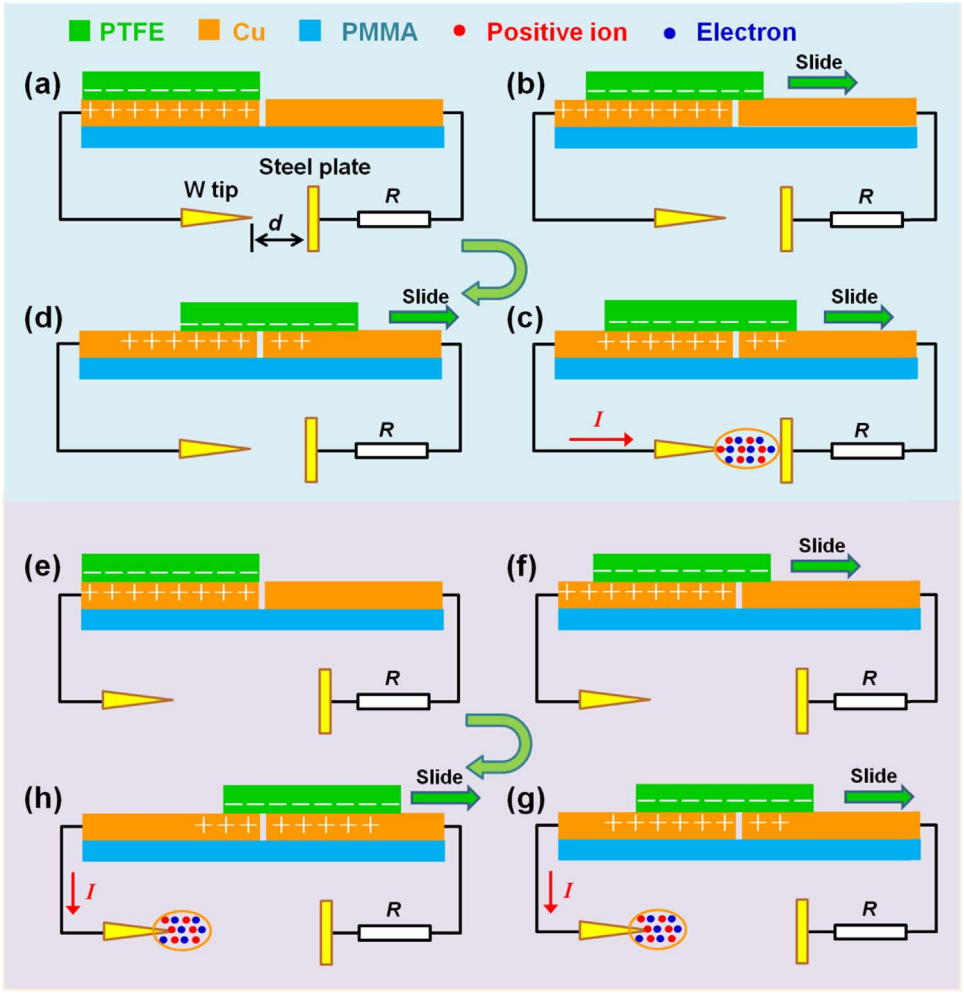

Fig. 1. The diagram of the working mechanism of the TENG-ADS. (a-d) The switch works in arc discharge mode with short *d*. (e-h) The switch works in corona discharge mode with long *d*.

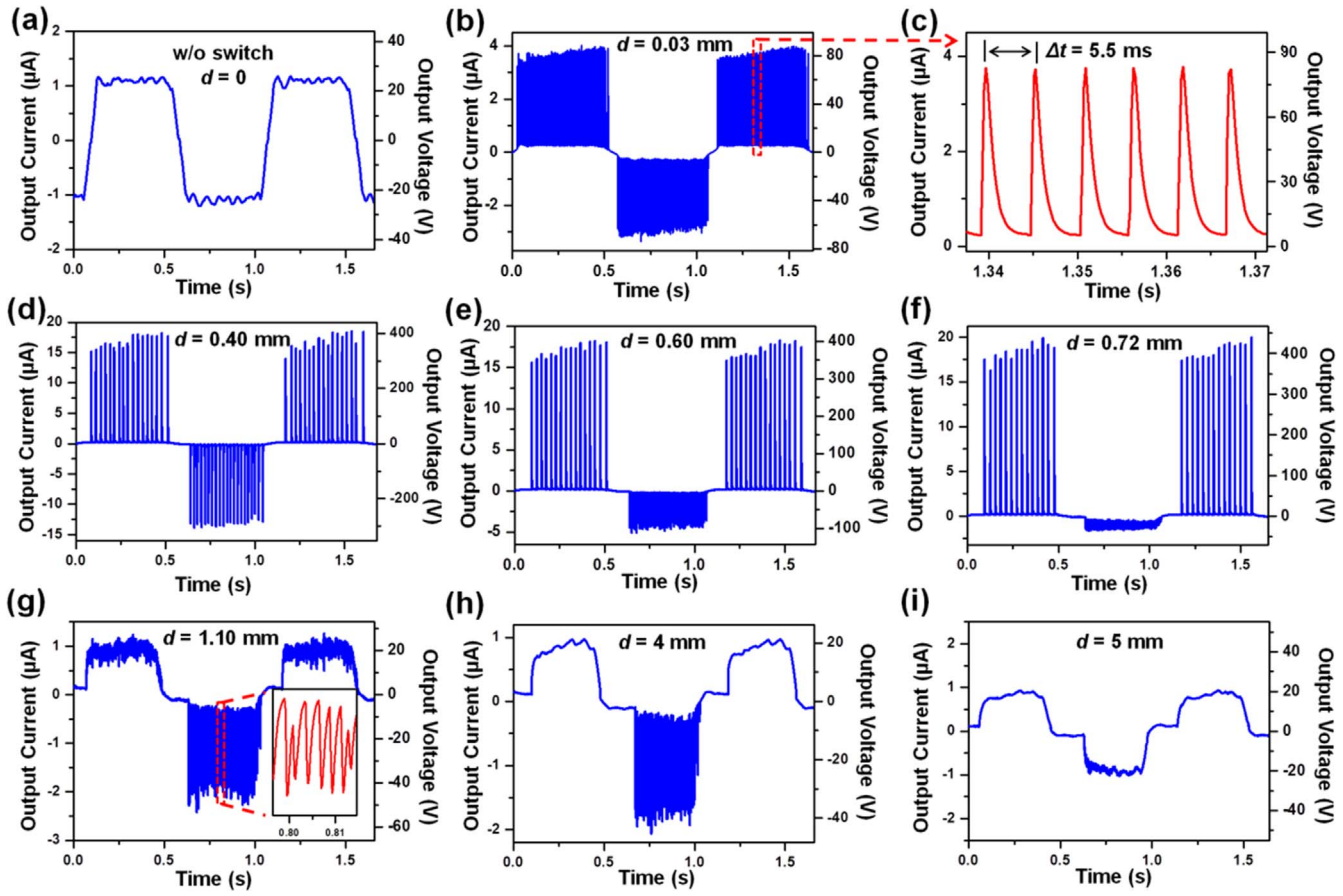

Fig. 2. The output current and voltage curves of the TENG-ADS for various *d*, where the load resistance is 22 MΩ. From (a) to (g), *d* increases from 0 to 5 mm. The amplification of (b) is shown as (c).

electrons and positive ions is generated and the air is electrically broken down. Recently, it has been reported that the TENG with high voltage can ionize organic molecules and protein through tip discharge, which can be applied in mass spectrometry as advanced ionization source [31]. For the TENG-ADS, only when the air gap of the switch is electrically broken down, the switch is closed and an electric output is generated.

For an air discharge process with a tip-plate electrodes configuration, there are two major discharge modes: the arc discharge and the corona discharge [30]. The electric field distribution in the air gap is a key factor for controlling its air discharge mode, which is largely dependent on tip-plate distance, *d*. Due to the enhancement of electric field by tip effect, the region around tip has stronger electric field. As *d* is short, the electric field distribution is relatively uniform, and the electric field around both tip and plate electrodes can reach the threshold value for air ionization. As a result, the generated plasma can directly bridge the two discharge electrodes to form a strong discharge process accompanied with bright arc, which is defined as an arc discharge [30]. For a long *d*, the electric field distribution in the air gap is largely non-uniform, and the electric field around the tip is much stronger due to the tip effect. As a result, only the air around the tip can be ionized, and the generated plasma is locally distributed around the tip, which cannot directly bridge the two discharge electrodes. This discharge process is defined as a corona discharge, which is a much weaker discharge process as compared with the arc discharge [32,33].

As the switch works in an arc discharge mode with short *d*, the working mechanism of the TENG-ADS is shown in Fig. 1a-d. In initial stage (Fig. 1a), the PTFE film overlaps with the left Cu electrode, and the negative triboelectric charges in PTFE film are balanced by the positive induction charges in the left Cu electrode. As the PTFE film slides rightwards (Fig. 1b), the negative charges in PTFE film and the positive charges in left Cu electrode are laterally separated, which causes potential difference between the two Cu electrodes. However, the potential difference is not high enough to induce air discharge, the switch is off, and the circuit is open. Therefore, there is no charge flowing between the two Cu electrodes during this process. As shown in Fig. 1c, as the PTFE film continues to slide rightward, the potential difference between the two Cu electrodes is increased to a threshold value for generating arc discharge. As a result, a plasma bridging the two discharge electrodes is formed, and the switch is closed. For reaching electrostatic equilibrium, the positive charges in left Cu electrode flow into right Cu electrode to generate a pulsed current, and the potential difference is reduced to zero. After that, the plasma is vanished, the switch is off again, and the circuit is open during the following rightward sliding process of the PTFE film (Fig. 1d). As the potential difference is increased to the threshold value for arc discharge again, another air discharge process will start to generate another current peak with same polarization. As the PTFE slides leftward, the opposite potential difference will be induced, and the current peak with opposite polarization will be generated.

As the switch works in a corona discharge mode with long *d*, the working mechanism of the TENG-ADS is shown in Fig. 1e-h. The former processes (Fig. 1e and f) are similar to that as the switch works in an arc discharge mode (Fig. 1a and b). As the potential difference is high enough to generate corona discharge, a local plasma around the tip is formed to generate current flow (Fig. 1g). However, the air gap cannot be directly bridged by the local plasma around the tip. In corona discharge process, charge transport process is dominated by the drift and diffusion of electrons and positive ions in the plasma, which is much slower than arc discharge [32]. Due to the slow charge transport

properties, the potential difference decreased by the corona discharge can be compensated by the increased potential caused by rightward sliding of the PTFE film. As a result, the switch is still on state as the PTFE film continues to slide rightward, and a persistent current is generated during this process (Fig. 1h). As the PTFE slides leftward, the opposite potential difference will be induced, and the current peak with opposite polarization will be generated.

The measured output current and voltage curves of the TENG-ADS for various d are shown in Fig. 2, where the external load resistance R is 22 MΩ and d is gradually increased from zero to 5 mm. These figures clearly show that the output performances of the TENG are largely modulated by changing d. As d is zero (Fig. 2a), the tip is in direct contact with the plate and the switch is always closed. Therefore, the TENG-ADS as d is zero becomes a traditional sliding TENG without a switch, which has typical output current and voltage curves like square wave [2]. The output current and voltage are 1.1 μA and 24.2 V, respectively. The positive and negative half cycles correspond to the rightward and leftward sliding processes of the PTFE film, respectively. Fig. 2b shows the output curves as d is 0.03 mm, in which multiple pulsed peaks appear in each half cycle. As shown in the magnification of the positive peaks (Fig. 2c), the interval between two peaks is 5.5 ms, and the corresponding frequency is 181.8 Hz. As d is 0.03 mm, the instantaneous output current and voltage peaks are about 3.7 μA and 81.4 V, respectively. As d is increased to 0.40 mm (Fig. 2d), the instantaneous output current and voltage peaks are increased to 16.8 μA and 369.6 V, respectively, and the interval time between the peaks is increased to 25.4 ms. As d is increased to 0.60 mm (Fig. 2e), the output peaks in positive half cycle become higher, however the output peaks in negative half cycle drop to about −4.5 μA and −99.0 V. As d is increased to 0.72 mm (Fig. 2f), the peaks in positive half cycle continue to increase, and the negative peak values continue to drop. As d is increased to 1.10 mm (Fig. 2g), the positive signals also drop to about 0.98 μA and 21.6 V. As shown in the magnification of negative signals (inset of Fig. 2g), there are irregular peaks with interval time about 2.4 ms. As d is increased to 4 mm (Fig. 2h), the positive irregular peaks are disappeared, and the positive current curves become smooth. As d is increased to 5 mm (Fig. 2i), the negative irregular peaks are disappeared, and the negative current curves become smooth.

The measurement results shown in Fig. 2 indicate that the electrical output performances of the TENG-ADS are largely dependent on d. In order to clearly show the variation tendency, the electrical output parameters at various d are plotted in Fig. 3, where the load resistance R is 22 MΩ. Fig. 3a and b show the dependence of instantaneous output current peak, voltage peak, and power peak on d for positive half cycle, and their semi-log plots are shown in the inset. The corresponding plots for negative half cycle are shown in Fig. 3c and d. Fig. 3e and f shows the dependence of output energy in a total cycle and transferred charge on d, respectively. Here, the total output energy is calculated by integrating I^2R during the time of an entire operation cycle of the TENG-ADS, which is the sum of the output energy in a positive half cycle and a negative half cycle. It is clear that the instantaneous current and voltage peaks, power peaks, total energy per cycle, and transferred charge are largely dependent on d. For example, the maximum instantaneous power peak in positive half cycle of 7.4 mW at $d = 0.72$ mm is 632 times higher than the minimum value of 11.7 μW at $d = 20$ mm. The maximum output energy per cycle of 172 μJ at $d = 0.40$ mm is 45 times higher than the minimum value of 3.8 μJ at $d = 20$ mm. For the output parameters in the positive half cycle (shown in Fig. 3a and b), there is an important turning point as d is 0.72 mm. Around this turning point, the instantaneous current peak, voltage peak, output power peak, and the total output energy per cycle are all sharply decreased. The instantaneous current peak drops from 18.3 μA to 0.8 μA, the voltage peak drops from 402.6V to 17.6 V, the instantaneous output power peak drops from 7.4mW to 0.04 mW, and the output energy per cycle drops from 97.1 μJ to 18.1 μJ. This turning point around 0.72 mm is attributed to the changing of the switch's working mode in the positive half cycle. As d is less and higher than 0.72 mm, the air discharge switch in positive half cycle works in the arc discharge mode and the corona changes mode, respectively. For the negative half cycle of the TENG-ADS (shown in Fig. 3c and d), there are two important turning point, which are appeared around 0.4 mm and 4 mm, respectively. The turning point around 0.4 mm also causes the drop of the total output energy in an entire cycle, as shown in Fig. 3e.

The working mode of the switch is determined by whether the generated plasma can bridge the two discharge electrodes. In the air discharge process, the reduced electric field E/N is a generally used parameter to determine whether the electrons can be accelerated to high enough energy to ionize air and generate plasma, where E is the electric field, N is the density of neutral molecule. It is calculated that the threshold value of E/N for generating plasma is about 80 Td, where Td is a unit of the reduced electric field, and 1 Td $= 10^{-21}$ Vm^2 [32]. Within the plasma region, E/N is larger than 80 Td, which is high enough to generate plasma. Outside the plasma region, E/N is lower than 80 Td, and the energy of the accelerated electrons is not high enough to ionize air. In the turning point between the arc discharge and the corona discharge, the reduced electric field E/N at the surface of the plate electrode equals 80 Td, and the radius of the plasma region equals d. For less d, the plasma can directly bridge the two discharge electrodes, and the switch works in an arc discharge mode. For larger d, the radius of the plasma region is less than d, and the switch works in a corona discharge mode. As shown in Fig. 2b-d, the output current and voltage curves at negative half cycle have smaller peaks than positive half cycle, which indicates that less threshold voltage is required for negative air discharge process (the tip is negatively biased). The less threshold voltage causes lower electric field distributed in the air gap, which reduces the radius of the generated plasma in negative half cycle. This is the reason why the turning point between the arc discharge and the corona discharge in negative half cycle (0.40 mm) is smaller than that in positive half cycle (0.72 mm).

As the switch works in an arc discharge mode, higher threshold voltage of air discharge is required for larger d. As a result, the output voltage peak is increased with d, which also causes the increase of the instantaneous current peak, instantaneous output power peak and total output energy in a cycle. As the switch works in a corona discharge mode, the threshold voltage of air discharge switch is also increased with d. However, with increasing d, the equivalent resistance of the switch will be largely increased [31], which causes the decrease of the output voltage peak, instantaneous current peak, instantaneous output power peak, and output energy in a cycle. In addition, there is another turning point as d is 4 mm in the negative half cycle, which not only causes the drop of current peak, voltage peak and power peak in the negative half cycle, but also causes the drop of output energy in an entire cycle. As shown in Fig. 2e-h, the irregular negative pulse peaks with a frequency about 416 Hz are appeared in the current and voltage curves, as d is in the range from 0.6mm to 4 mm, which is attributed to the generation of Trichel pulse in the negative corona discharge process with higher electric field [33]. As d is increased to 5 mm (Fig. 2i), the irregular negative peaks are almost disappeared, and the curve become smooth, which causes the turning point around 4 mm in the negative half cycle. For the transferred charge plot shown in Fig. 3f, as d is less than 2.3 mm, the total transferred charge values are about 502 nC, which don't change with d. As d is increased from 2.3 to 20 mm, the transferred charge is gradually decreased from 502 nC to 190 nC. With the increase of d, the threshold voltage for turning on the air discharge switch is increased. Close to the final process of each half cycle, the potential difference between two electrodes is less than the threshold voltage, and the switch is open. As a result, the left charges cannot be transferred between the two electrodes, which causes the decrease of the total transferred charges in larger d. However, as d is less than 2.3 mm, the total transferred charge doesn't decrease with d. The ions in the plasma region may remain some time for relaxation, after the potential difference is lower than the threshold voltage of the air

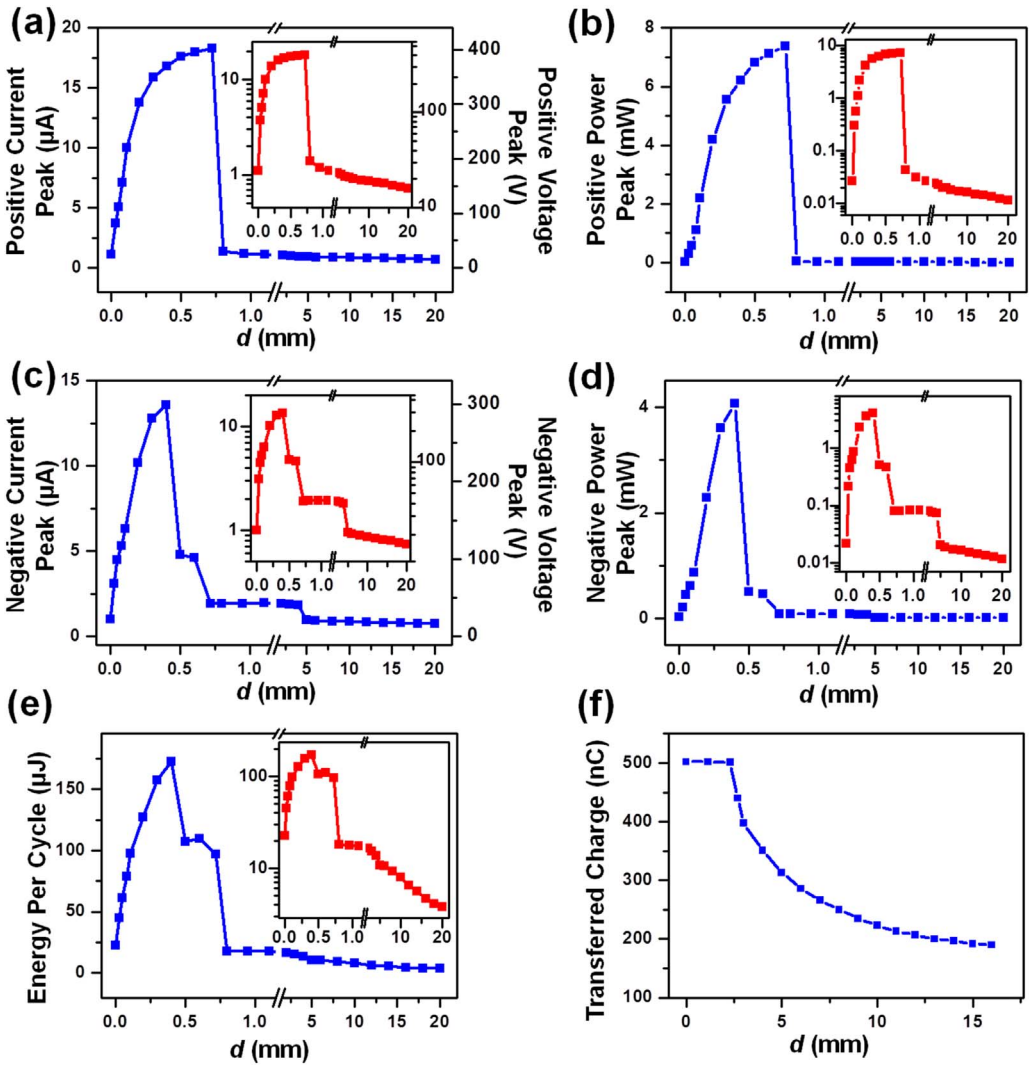

Fig. 3. The dependence of instantaneous current peak, voltage peak, and power peak on d in positive half cycle (a-b) and negative half cycle (c-d). The dependence of output energy in an entire cycle (e) and transferred charge (f) on d. The insets show the corresponding plots in semi-log scale.

discharge process. These phenomena may be caused by the left ions in the plasma region. While, the deeper mechanism of this phenomena need further investigation.

It has been reported previously that the electrical output performances of TENG on lower load resistance could be largely improved by using a switch [21]. For the TENG-ADS in this experiment, the electrical output performances for various R are measured and demonstrated in Fig. 4. Fig. 4a shows the current curves for three different R values (2 MΩ, 200 MΩ, and 4 GΩ) as the switch works in an arc discharge mode (d = 0.20 mm). For clear presentation, the current curves for 200 MΩ and 4 GΩ are magnified 10 and 20 times, respectively. For the TENG with a switch, the output current is dominated by the external load resistance, and the higher load resistance leads to slower current transport process, which results in lower current peak and wider peak width [21]. For this reason, as R is increased from 2 MΩ to 4 GΩ, the current peaks become lower and wider, as shown in Fig. 4a. As R is 2 MΩ, separated current peaks are formed, and each current peak represents an arc discharge process. As R is 200 MΩ, two arc discharge processes are almost connected together. As R is increased to 4 GΩ, the last discharge process has not completed at the beginning of the next discharge process, and the current peak is increased step by step. In these curves, the peak patterns in the positive side and negative side are different, the positive current peaks are higher than the negative current peaks, and the negative current peaks have higher frequency, which is because the positive and negative current are attributed to the positive arc discharge and negative arc discharge processes of the air discharge switch, respectively.

Fig. 4b-e show the plots of electrical output parameters for various R ranging from 10 kΩ to 10 GΩ. The performances of the TENG-ADS as the switch works in the arc discharge mode and the corona discharge mode are represented by d = 0.20 mm and d = 5 mm, respectively. For comparison, the performances of the same TENG without a switch are also measured and plotted. The energy values plotted in Fig. 4e is the total output energy on a load resistance R in an entire operation cycle of the TENG, which is calculated by integrating I^2R in the operation cycle. Compared with the TENG without a switch, the TENG-ADS in the corona discharge mode has slightly higher instantaneous current peaks and instantaneous output power peaks, almost equal voltage peaks, and slightly lower output energy. As R is 1 MΩ, the instantaneous current peak and instantaneous output power peak of the TENG-ADS are 20% and 44% higher than the TENG without a switch, and its total output energy in an operation cycle is 45% lower than the TENG without a switch. The output energy is determined by the product of the output voltage and the transferred charge [26]. As shown in Fig. 3d, the transferred charge at d = 5 mm is 38% lower than that at d = 0 mm, which causes the lower output energy of the TENG-ADS in the corona discharge mode.

As the TENG-ADS works in the arc discharge mode (d = 0.20 mm), its instantaneous current peak, voltage peak, instantaneous output power peak and total output energy are almost equal to the TENG without a switch, as R is in the range from 400 MΩ to 4 GΩ. As R is lower than 400 MΩ, the performances of TENG-ADS are significantly

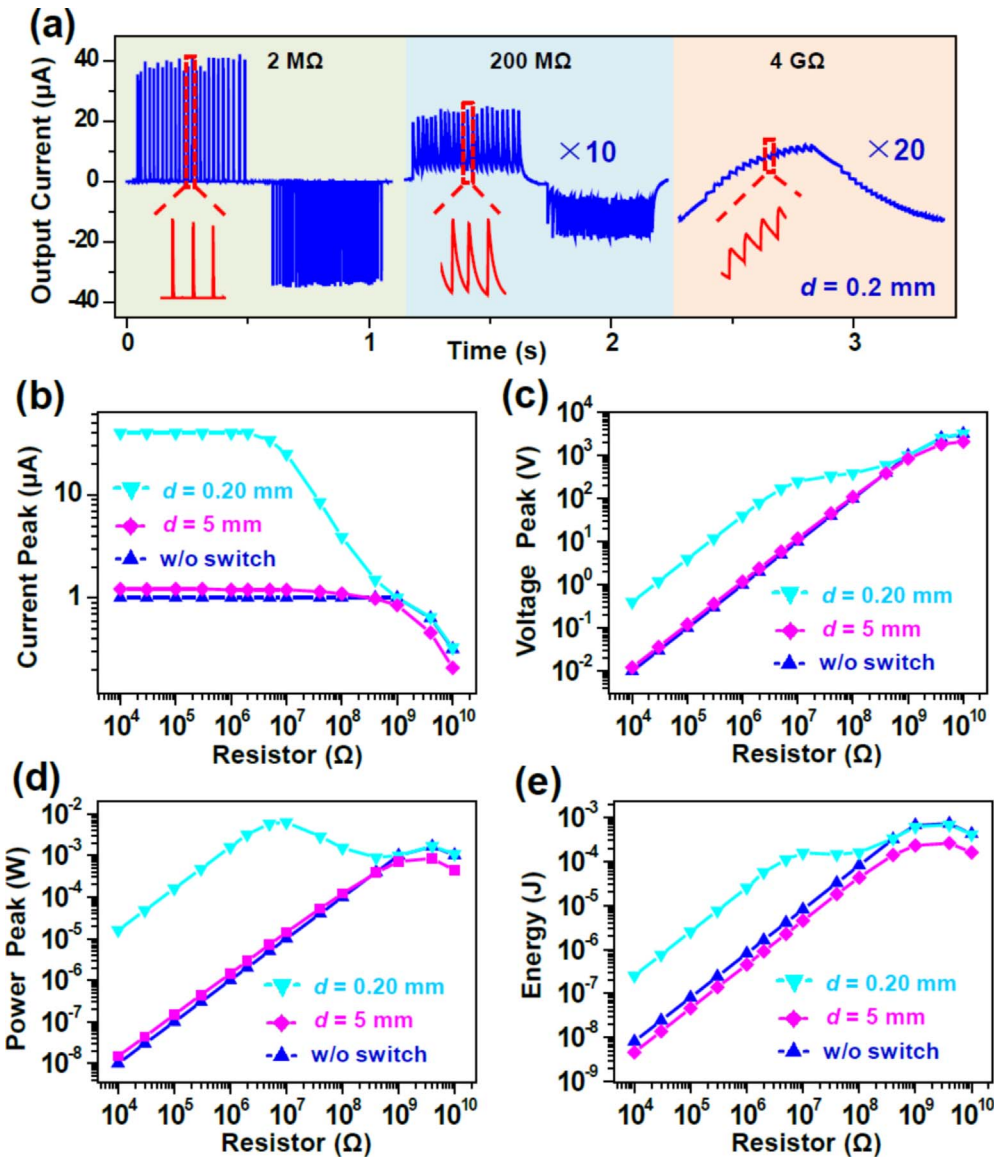

Fig. 4. (a) The output current curves for various load resistances of the TENG-ADS, where d is 0.20 mm and the switch works in arc discharge mode, and the current curves for 200 MΩ and 4 GΩ are amplified for 10 and 20 times, respectively. The dependence of instantaneous current peaks (b), voltage peaks (c), instantaneous power peaks (d) and output energy per cycle (e) on load resistances as the switch works in arc discharge mode (d = 0.20 mm), corona discharge mode (d = 5 mm), and direct contact mode (d = 0), respectively.

better than the TENG without a switch. As shown in Fig. 4b, the instantaneous current peak of the TENG without a switch is 1.0 μA as R is 400 MΩ, and does not continue to increase as R is decreased from 400 MΩ to 10 kΩ. For the TENG-ADS, the instantaneous current peak is increased from 1.5 μA to 40 μA as R is decreased from 400 MΩ to 2 MΩ, and does not continue to increase as R is decreased from 2 MΩ to 10 kΩ. Compared with the same TENG without a switch as R is lower than 2 MΩ, the instantaneous current peak, voltage peak, instantaneous output power peak and output energy of the TEGN-ADS are increased by 40, 40, 1600 and 31 times, respectively. The enhancement of instantaneous output power peak and total output energy is an important advantage of the TENG with a switch [20–26]. Through establishing the standards and figure-of-merits of the TENG by theoretical calculation, it is pointed out that the output energy is dependent on the maximum output voltage of the TENG, and the output energy can only be maximized by using a switch [22]. Using a switch, the output voltage can almost reach the open-circuit voltage of the TENG, which largely enhances the output energy of the TENG, especially for load resistances lower than 1 MΩ [21–25]. For an ideal switch, the equivalent resistance of the switch is zero, and the output voltage and output energy for the TENG with a switch is a constant, which doesn't vary with the external load resistance. Different with previous switches triggered by either mechanical motion [21,23–26] or circuit [20,27,28], the air discharge switch has an equivalent resistance, since the air discharge process is driven by high voltage which will cause energy consumption [34]. As shown in the current plots in Fig. 4b, the output current of the TENG-ADS in the arc discharge mode and the corona discharge mode cannot continue to increase as R is lower than 2 MΩ and 400 MΩ, respectively. This means that the equivalent resistances of the arc discharge switch and the corona discharge switch are about 2 MΩ and 400 MΩ, respectively. Due to the existence of the equivalent resistance in this switch, the voltage peak, instantaneous output power peak, and total output energy of the TENG-ADS are linearly reduced as R is lower than the equivalent resistance of the switch, as shown in Fig. 4c-e. However, in spite of existing equivalent resistance in the air discharge switch, the output power and energy of the TENG-ADS in the arc discharge mode are remarkably enhanced as R is lower than 400 MΩ, compared with the same TENG without a switch.

According to the results and discussions above, the output performances of the TENG-ADS are largely dependent on the working mode of the air discharge switch. Besides d, it is found that the UV light can also modulate the working mode of the switch and the output current of the TENG-ADS. As shown in Fig. 5a, the output current of the TENG-ADS is largely decreased as the UV light is illuminated, where d is 0.72 mm, R

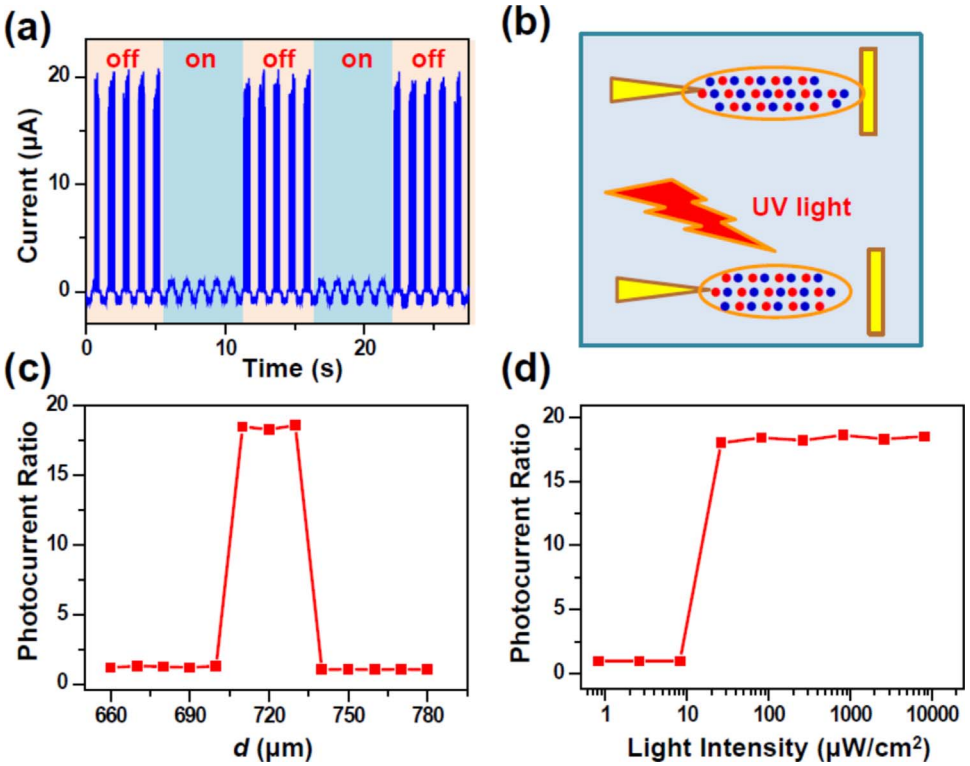

Fig. 5. (a) The output current curves of the TENG-ADS as the UV light is turned on and off for multiple cycles. (b) The diagram of the changing of the switch's working mode from arc discharge to corona discharge induced by UV light. (c) The dependence of current ratio on *d*. (d) The dependence of current ratio on light intensity.

is 22 MΩ, and the central wavelength and light intensity of the UV light are 365 nm and 8.2 mW/cm^2, respectively. As the TENG-ADS operates in dark condition, the switch works in the arc discharge mode, and the pulsed output current peaks around 19 μA are generated. As the UV light is turned on, the pulsed current peaks are disappeared and the current is decreased to about 1 μA, which means the switch is changed from the arc discharge mode to the corona discharge mode. The diagram of the mechanism of this UV light photodetector is shown in Fig. 5b. During the measurement of the photocurrent properties, *d* is selected as 0.72 mm, which is around the turning point between the arc discharge mode and the corona discharge mode. In this case, the radius of the plasma region in dark condition equals *d*. Since the UV light can produce extra electrons and positive ions in air, the threshold voltage of the air discharge will be decreased [35]. The less threshold voltage will decrease both the reduced electric field *E/N* distributed in the air gap and the radius of the generated plasma. Therefore, under UV light, the radium of the plasma region is decreased and becomes smaller than *d*, which changes the switch from the arc discharge mode to the corona discharge mode. As mentioned above, the equivalent resistant of the corona discharge (about 400 MΩ) is much larger than that of the arc discharge (about 2 MΩ), therefore the output current of the TENG-ADS is decreased under UV light. Here, it is noted that the UV light does not change the performance of the TENG itself, but only changes the plasma generation behaviors around the tip and the corresponding equivalent resistance of the air discharge switch.

As shown in Fig. 5c, the high current ratio about 18.2 between dark and UV light can only be obtained in a narrow range of *d* from 0.71mm to 0.73 mm, which is around the turning point between the arc discharge mode and the corona discharge mode. This result also verifies that the mechanism of this TENG-ADS-based UV light photodetector is attributed to the changing of the switch from the arc discharge mode to corona discharge mode. Fig. 5d shows the dependence of current ratio on light intensity, where *d* is 0.72 mm. As the light intensity reaches 26.2 μW/cm^2, the current ratio is sharply increased from 1.2 to 18.2, and no longer continues to increase with light intensity. This means that the light intensity of 26.2 μW/cm^2 is the threshold value for changing the working mode of the switch. The response and recovery speed of the photodetector are limited by two factors, one is the photo-response of the air discharge process, the other is the operation frequency of the TENG. A control experiment was carried out to test the response and recovery speed of the air discharge process, where a constant voltage of 1.9 kV was applied between tip and plate, and the tip-plate distance is 2 mm. As shown in Fig. S3 in supporting information, the response and recovery time of the photo-response of the air discharge process are 51 ms and 43 ms, respectively. This means that for a TENG with an operation frequency lower than 20 Hz, the response and recovery speed are limed by the operation of TENG, but not by the photo-response of the air discharge process. The operation of this photodetector is based on changing the output current of the TENG-ADS itself, and no extra power source is required, which can be used as an active self-powered UV light photodetector. Unlike most other photodetectors [13,36–38], the output current and output power of this UV light photodetector are decreased under UV light, but not increased. This unique characteristic has potential applications in low power photodetector, inverse photoconductivity, inverse optical-controlled logic circuit, and so on.

3. Conclusion

In this paper, a self-powered air discharge switch is developed for a sliding TENG. Only as the output voltage of the TENG is high enough for inducing air discharge, the switch is closed and an electrical output is generated. With the increase of the distance between the two discharge electrodes, the switch is changed from the arc discharge mode to the corona discharge mode. Compared with the same TENG without a witch, the output performances of the TENG with an arc discharge switch are largely enhanced in lower load resistances. The instantaneous output power peak at each tip discharge and the total output energy in a TENG's operation cycle are increased by 1600 times and 31 times, respectively, as the external load resistance is lower than 2 MΩ. Also, it is found that the UV light can change the switch from the arc discharge mode to the corona discharge mode, the equivalent resistance of the switch is increased, and the output current of the TENG-ADS is decreased. Based on this phenomenon, an active self-powered UV light photodetector is developed. The TENG with an air discharge

switch provides a promising route for managing the TENG's output power and developing the self-powered UV light sensors.

4. Experimental section

4.1. The preparation of the TENG-ADS

The TENG used in this paper worked in a sliding mode. Two square Cu films were deposited on a PMMA substrate by a PVD deposition system with a shadow mask. The thickness and length of the Cu film are 100 nm and 5 cm, respectively, and the distance between two Cu film is 1 mm. A square PTFE film adhered to a PMMA substrate was used as the triboelectric layer of the TENG. The thickness and length of the PTFE film are 100 μm and 5 cm, respectively. The surface of the PTFE film was treated by reactive ion etching in 30 s to enhance its triboelectric performance. For the air discharge switch, a W tip with a curvature radius of 15 μm and a stainless steel plate are electrically connected with the two Cu electrodes of TENG, respectively. The steel plate is rectangular with a length and width of 6 cm and 2 cm, respectively. The W tip is perpendicular to the steel plate, and the distance between them, *d*, is precisely controlled by a micro-manipulation stage.

4.2. The characterization of the TENG-ADS

The operation and characterization of the TENG-ADS were carried out in air atmosphere and room temperature. The electrical outputs of the TENG-ADS were measured using a programmable multi-functional electrometer (Keithley, Model 6514) and a low-noise current pre-amplifier (Stanford Research System, Model SR570). A 300 W Xenon lamp equipped with an UV light band pass filter was used as the UV light source, where the central wavelength and bandwidth of the filter are 365 nm and 30 nm, respectively. The output power of the UV light source was measured using an optical power meter (Newport, Model 1916C). The neutral attenuator filters were used to modulate the light intensity.

Acknowledgements

Supports from the National Natural Science Foundation of China (61522405), the Program for Changjiang Scholars and Innovative Research Team in Chinese University (PCS IRT_15R18), the National Key R & D Project from Minister of Science and Technology of China (2016YFA0202704), and the Scientific and Technological Innovation Team in University of Henan Province (15IRTSTHN009) are appreciated.

Appendix A. Supporting information

Supplementary data associated with this article can be found in the online version at http://dx.doi.org/10.1016/j.nanoen.2017.11.062.

References

[1] F.R. Fan, Z.Q. Tian, Z.L. Wang, Nano Energy 1 (2012) 328–334.
[2] Z.L. Wang, J. Chen, L. Lin, Energy Environ. Sci. 8 (2015) 2250–2282.
[3] G. Zhu, Y.S. Zhou, P. Bai, X.S. Meng, Q. Jing, J. Chen, Z.L. Wang, Adv. Mater. 26 (2014) 3788–3796.
[4] L. Lin, S.H. Wang, Y.N. Xie, Q.S. Jing, S.M. Niu, Y.F. Hu, Z.L. Wang, Nano Lett. 13 (2013) 2916–2923.
[5] J. Yang, J. Chen, Y. Yang, H.L. Zhang, W.Q. Yang, P. Bai, Y.J. Su, Z.L. Wang, Adv. Energy Mater. 4 (2014) 1–9.
[6] W. Xu, L.B. Huang, J.H. Hao, Nano Energy 40 (2017) 399–407.
[7] Y. Yang, G. Zhu, H.L. Zhang, J. Chen, X.D. Zhong, Z.H. Lin, Y.J. Su, P. Bai, X.N. Wen, Z.L. Wang, ACS Nano 7 (2013) 9461–9468.
[8] L.B. Huang, W. Xu, G.X. Bai, M.C. Wong, Z.B. Yang, J.H. Hao, Nano Energy 30 (2016) 36–42.
[9] Y.N. Xie, S.H. Wang, S.M. Niu, L. Lin, Q.S. Jing, Y.J. Su, Z.Y. Wu, Z.L. Wang, Nano Energy 6 (2014) 129–136.
[10] Z.H. Lin, G. Cheng, S.M. Lee, K.C. Pradel, Z.L. Wang, Adv. Mater. 26 (2014) 4690–4696.
[11] J. Chen, J. Yang, Z.L. Li, X. Fan, Y.L. Zi, Q.S. Jing, H.Y. Guo, Z. Wen, K.C. Pradel, S.M. Niu, Z.L. Wang, ACS Nano 9 (2015) 3324–3331.
[12] G. Zhu, Y.J. Su, P. Bai, J. Chen, Q.S. Jing, W.Q. Yang, Z.L. Wang, ACS Nano 8 (2014) 6031–6037.
[13] Z.H. Lin, G. Cheng, Y. Yang, Y.S. Zhou, S.M. Lee, Z.L. Wang, Adv. Funct. Mater. 24 (2014) 2810–2816.
[14] Z. Wen, Q.Q. Shen, X.H. Sun, Nano-Micro Lett. 9 (45) (2017) 1–19.
[15] H.L. Zhang, Y. Yang, Y.J. Su, J. Chen, C.G. Hu, Z.K. Wu, Y. Liu, C.P. Wong, Y. Bando, Z.L. Wang, Nano Energy 2 (2013) 693–701.
[16] Z.H. Lin, G. Zhu, Y.S. Zhou, Y. Yang, P. Bai, J. Chen, Z.L. Wang, Angew. Chem-Int. Ed. 52 (2013), pp. 5065–5069.
[17] L.B. Huang, G.X. Bai, M.C. Wong, Z.B. Yang, W. Xu, J.H. Hao, Adv. Mater. 28 (2016) 2744–2751.
[18] W. Xu, L.B. Huang, M.C. Wong, L. Chen, G.X. Bai, J.H. Hao, Adv. Energy Mater. 7 (2017) 1601529.
[19] S.H. Wang, L. Lin, Y.N. Xie, Q.S. Jing, S.M. Niu, Z.L. Wang, Nano Lett. 13 (2013) 2226–2233.
[20] S.M. Niu, X.F. Wang, F. Yi, Y.S. Zhou, Z.L. Wang, Nat. Commun. 6 (2015) 8975.
[21] G. Cheng, Z.H. Lin, L. Lin, Z.L. Du, Z.L. Wang, ACS Nano 7 (2013) 7383–7391.
[22] Y.L. Zi, S.M. Niu, J. Wang, Z. Wen, W. Tang, Z.L. Wang, Nat. Commun. 6 (2015) 8376.
[23] Y.F. Li, G. Cheng, Z.H. Lin, J. Yang, L. Lin, Z.L. Wang, Nano Energy 11 (2015) 323–332.
[24] G. Cheng, L. Zheng, Z.H. Lin, J. Yang, Z.L. Du, Z.L. Wang, Adv. Energy Mater. 5 (2015) 1–9.
[25] G. Cheng, Z.H. Lin, Z.L. Du, Z.L. Wang, Adv. Funct. Mater. 24 (2014) 2892–2898.
[26] Y.L. Zi, J. Wang, S.H. Wang, S.M. Li, Z. Wen, H.Y. Guo, Z.L. Wang, Nat. Commun. 7 (2016) 0987.
[27] F.B. Xi, Y.K. Pang, W. Li, T. Jiang, L.M. Zhang, T. Guo, G.X. Liu, C. Zhang, Z.L. Wang, Nano Energy 37 (2017) 168–176.
[28] X.L. Cheng, L.M. Miao, Y. Song, Z.M. Su, H.T. Chen, X.X. Chen, J.X. Zhang, H.X. Zhang, Nano Energy 38 (2017) 438–446.
[29] D.K. Davies, J. Phys. D. Appl. Phys. 2 (1969) 1533–1537.
[30] M.J. Rycroft, J. Atmos. Terr. Phys. 1993 (55) (1993) 1487.
[31] A.Y. Li, Y.L. Zi, H.Y. Guo, Z.L. Wang, F.M. Fernández, Nat. Nanotechnol. 12 (2017) 481–487.
[32] J.H. Chen, J.H. Davidson, Plasma Chem. Plasma Process. 23 (2003) 83–102.
[33] R. Morrow, Phys. Rev. A. 32 (1985) 1799–1809.
[34] L.M. Vasilyak, S.P. Vetchinin, D.N. Polyakov, Tech. Phys. Lett. 25 (1999) 749–751.
[35] W.J. Zhou, H. Li, X. Yi, J. Tu, J.H. Yu, IEEE Trans. Dielectr. Electr. Insul. 18 (2011) 232–237.
[36] L. Duan, F.N. He, Y. Tian, B. Sun, J.B. Fan, X.C. Yu, L. Ni, Y. Zhang, Y.N. Chen, W.X. Zhang, ACS Appl. Mater. Interfaces 9 (2017) 8161–8168.
[37] G. Cheng, X.H. Wu, B. Liu, B. Li, X.T. Zhang, Z.L. Du, Appl. Phys. Lett. 99 (2011) 30–32.
[38] S.C. Rai, K. Wang, Y. Ding, J.K. Marmon, M. Bhatt, Y. Zhang, W. Zhou, Z.L. Wang, ACS Nano 9 (2015) 6419–6427.

Gang Cheng received the B.S. degree from Henan University in 2000 and the Ph.D. degree from Jilin University in 2008. He was a visiting scholar in School of Materials Science and Engineering at Georgia Institute of Technology under the supervision of Prof. Zhong Lin (Z. L.) Wang from 2013 to 2016. Currently, he is a full-time professor at the key laboratory for special functional material, ministry of education, Henan University, Kaifeng, China. His research interests are nanostructure-based electronic and optoelectronic devices, nanogenerator, and self- powered nanosensors.

Hai Wu Zheng received his Ph.D. degree from the University of Science and Technology of China (USTC) in 2006. Then he joined the School of Physics and Electronics of Henan University. Currently, he is a full-time professor at Henan Key Laboratory of Photovoltaic Materials, School of Physics and Electronics, Henan University. His current research interests mainly include triboelectric nanogenerators, photovoltaic effects of ferroelectric and piezoelectric thin films/nanowires.

Feng Yang is a Ph. D candidate in the key lab of Ministry of education for special functional materials and a lecturer in the school of physics and electronics of Henan University. He received the B.S. degree from Henan University in 2003. His research interests are nanostructure-based electronic and optoelectronic devices.

Lei Zhao received the B.S. degree from Northwest Normal University in 2003 and the master degree from Henan University in 2011. He is currently a Ph.D. student at the key laboratory for special functional material, ministry of education, Henan University, under the supervision of Prof. Gang Cheng. His research interests are nanostructure-based electronic and optoelectronic devices, self- powered nano-sensors.

Mingli Zheng received the B.S. degree from the Xinyang Normal University, Xinyang, in 2015. He is currently pursuing the master degree at the key laboratory for special functional material, ministry of education, Henan University, Kaifeng, China. His research interests mainly include design and fabrication of ZnO nanowire film UV detector and TENG air discharge.

JunjieYang received the B.S. degree in Chemistry Education from Shandong University of Technology, China, in 2016. She is currently pursuing the master degree at Key Lab for Special Functional Materials, Ministry of Education, Henan University, China. Her research is focusing on output power management of the triboelectric nanogenerator.

Huaifang Qin received his B.S. degree in Material Forming and Control Engineering from Shenyang Ligong University, China in 2016. He is currently pursuing his undergraduate degree in Henan University. His research interests are mainly focused on triboelectric nanogenarator and self-powered Sensor system, especially focus on the power management and their applications in sensor networks.

Zuliang Du received the Master's degree (1991) and Ph.D. degree (1999) in Condensed Matter Physics from Jilin University. Now, he is director of Key Lab for Special Functional Materials of Ministry of Education, Henan University. His major is condensed matter physics and materials and his main interest is concerned with the research of nanostructures materials and devices, photoelectric materials and molecule assembly. Up to date, there are more than 10 national-level research projects in total completed or being undertaken, including those from the National Key Projects for Basic Researches of China (973-project), the National High-Tech Programmes of China (863-Programmes), and the projects from the National Natural Science Foundation of China (NSFC).

Prof. Zhong Lin (Z.L.) Wang received his Ph.D. from Arizona State University in physics. He now is the Hightower Chair in Materials Science and Engineering, Regents' Professor, Engineering Distinguished Professor and Director, Center for Nanostructure Characterization, at Georgia Tech. Dr. Wang has made original and innovative contributions to the synthesis, discovery, characterization and understanding of fundamental physical properties of oxide nanobelts and nanowires, as well as applications of nanowires in energy sciences, electronics, optoelectronics and biological science. His discovery and breakthroughs in developing nanogenerators established the principle and technological road map for harvesting mechanical energy from environment and biological systems for powering a personal electronics. His research on self-powered nanosystems has inspired the worldwide effort in academia and industry for studying energy for micro-nano-systems, which is now a distinct disciplinary in energy research and future sensor networks. He coined and pioneered the field of piezotronics and piezo-phototronics by introducing piezoelectric potential gated charge transport process in fabricating new electronic and optoelectronic devices. Details can be found at:www.nanoscience.gatech.edu.